Dynamic interaction patterns of oblique detonation waves with boundary layers in hypersonic reactive flows

Jie Sun [a], Pengfei Yang [a,b,*], Zheng Chen [a]

[a] HEDPS, CAPT, SKLTCS, College of Engineering, Peking University, Beijing 100871, China
[b] State Key Laboratory of High Temperature Gas Dynamics, Institute of Mechanics, Chinese Academy of Sciences, Beijing 100190, China

ARTICLE INFO

ABSTRACT

Due to their high thermal cycle efficiency and compact combustor, oblique detonation engines hold great promise for hypersonic propulsion. Previous numerical simulations of oblique detonation waves have predominantly solved the Euler equations, disregarding the influence of viscosity and boundary layers. This work aims to study how the interaction between the oblique detonation wave and the boundary layer influences the detonation wave structures in confined spaces. Two-dimensional numerical simulations considering detailed chemistry are performed in a stoichiometric H_2/air mixture. The results indicate that the wedge-induced oblique detonation wave generates a strong adverse pressure gradient upon impacting the upper wall, leading to boundary layer separation. The separation zone subsequently induces an oblique shock wave near the upper wall, and an increase in separation angle will cause the transition from an oblique shock wave to an oblique detonation wave. The formation of the separation zone reduces the actual flow area and may even lead to flow choking; its obstructive effect is similar to that of the Mach stem in inviscid flow. To establish a connection between the viscous recirculation zone and the inviscid Mach stem, we introduce a dimensionless parameter, η, based on the inviscid assumption. It is defined as the ratio of the inviscid Mach stem height to the channel entrance height. This parameter can be used to identify three wave systems in a viscous flow field: separation shock-dominated wave systems, separation detonation-dominated wave systems, and unstable Mach stem-dominated wave systems. Among these, the appearance of detonation Mach stems leads to flow choking, and the shock-detonation wave system continually moves upstream, ultimately causing the failure of the oblique detonation combustion. The findings of this study provide new insights into the investigation of the influence of viscosity on the flow structure of oblique detonation waves.

1. Introduction

Detonation is characterized by the coupling of shock waves and chemical reactions [1]. Operating close to constant-volume combustion, detonation offers higher thermal efficiency compared to traditional constant-pressure combustion [2]. Consequently, detonation holds significant potential in advanced combustion technologies [3–5]. The oblique detonation wave (ODW) shows promise for advanced hypersonic engines due to its self-sustained features and compact combustion chamber structure [6,7], which has attracted considerable interest among researchers.

Extensive studies have explored the influence of factors such as inflow Mach number, attack angle, and fuel state on ODW structures [8–12]. However, most studies neglect the effect of mixture viscosity since it is generally considered insignificant in detonation simulations [13–15]. The boundary layer attaching the wedge wall may affect the ODW structure, potentially resulting in novel conclusions different from those derived under inviscid conditions.

Recognizing this, researchers have numerically assessed the influence of the boundary layer on ODW structures. Oran et al.'s work [16, 17] indicated that the boundary layer effects can shorten the induction zone of the ODW, thereby accelerating detonation initiation. The boundary layer is observed to increase the ODW angle [16,17]. Fang et al. [18] focused on the influence of the boundary layer on ODW structures under different inflow Mach number conditions. Their results highlighted that for the abrupt ODW (corresponding to low inflow Mach numbers), the interaction between the reflected shock and the boundary layer forms a recirculation zone, as corroborated by recent

---

investigations [19–21]. However, for the smooth ODW (corresponding to high inflow Mach numbers), no recirculation zone is observed because the reflected shock originated from the initiation zone is too weak.

The influence of the boundary layer on ODW structures can be summarized in two points. Firstly, the boundary layer facilitates auto-ignition of the mixture near the wall, reducing the detonation initiation distance. Secondly, the reflected shock wave interacts with the boundary layer, inducing the recirculation zone near the wall. However, the main ODW structure is not significantly changed by the boundary layer effects. This is attributed to the fact that the ODW is induced by the wedge in a semi-open space and does not directly interact with the boundary layer.

In a limited space, the ODW directly impacts the wall, and the interaction between shock/detonation wave and the wall becomes significant. Wang et al. [22,23] and Zhang et al. [24] separately found that a Mach stem forms under inviscid condition when the ODW reflects on the wall, and the pressure ratio across the Mach stem can reach up to about 50. However, when the mixture viscosity is considered, i.e., there is a boundary layer on the wall, such a high pressure gradient may induce flow separation [25–27] and the interaction between the ODW and the boundary layer cannot be ignored. Relevant studies [28,29] have shown that direct interaction between the shock/detonation wave and the boundary layer will cause a series of separation bubbles and oblique shock waves (OSWs). Chen et al.'s studies [30,31] furtherly revealed that considering viscosity in numerical simulations results in better agreement with experimental observations for the flow separation phenomena caused by shock wave/boundary layer interactions. This raises the question of whether the Mach stem, observed under inviscid conditions, can still exist near a viscous wall when an ODW reflects off the wall. Furthermore, the influence of the boundary layer on the ODW structures within a confined combustor, as well as the relationship between viscous and inviscid detonation wave systems, has not been thoroughly explained or addressed. Given the significance of this research for both understanding shock/detonation dynamics and the application of advanced engines based on ODWs, this study is conducted.

The present work aims to investigate how the interaction between the ODW and the boundary layer influences the flow structures in confined spaces. Two-dimensional numerical simulations considering detailed chemistry are performed in a stoichiometric H_2/air mixture. Initially, the steady ODW under inviscid conditions is simulated as a reference. Subsequently, the mixture viscosity is considered, and the influence of ODW/boundary layer interactions on the flow structures is assessed under different wedge angles, Mach numbers and wall temperatures. Finally, the typical combustion modes are summarized, and the dynamic mechanisms are analyzed.

2. Model and numerical methods

The computational model is depicted in Fig. 1. The mixture enters the combustion chamber from *AD*, whose height is denoted as *H*. *CE* represents the outlet of the combustion chamber. Upon reviewing the simulation results, we observe that the majority of the flow at the outlet is supersonic. Conseq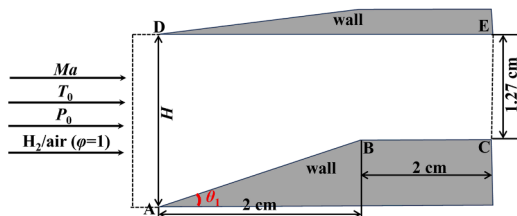uently, the outlet is modeled using the zero-gradient boundary condition. Additionally, the outlet is positioned far away from the location where the ODW reflects on the upper wall, with the aim of minimizing the influence of the outlet boundary on the upstream flow characteristics. *AB* corresponds to the wedge wall designed to induce the ODW, while *BC* and *DE* are the other walls. By default, the walls are modeled as adiabatic. Additionally, the influences of the wall temperatures (400 K, 1200 K, and 2000 K) on the simulation results are also evaluated in this paper. A segment of the free flow region is set ahead of the leading edges of both the upper and lower walls. This configuration ensures that the motions of the separation zones are not blocked by the left boundary. The stoichiometric H_2/air mixture at $T_0 = 400$ K and $P_0 = 1$ atm is used as the inflow, and the reaction mechanism proposed by Burke et al. [32] is employed to describe the hydrogen combustion process. The compression effects of the intake on the inflow are ignored and the mixture is assumed to be homogeneous. The inflow Mach number (*Ma*) ranges from 7 to 8.5, while the wedge angle (θ_1) varies from 20° to 30°

The Navier-Stokes equations are used to solve the flow problem above. The corresponding expressions are presented as [33]

$$\frac{\partial \rho}{\partial t} + \nabla \cdot (\rho V) = 0 \tag{1}$$

$$\frac{\partial (\rho V)}{\partial t} + \nabla \cdot (\rho VV) = -\nabla P + \nabla \cdot \tau \tag{2}$$

$$\frac{\partial (\rho E)}{\partial t} + \nabla \cdot [(\rho E + P)V] = -\nabla \cdot q + \nabla \cdot (V \cdot \tau) \tag{3}$$

$$\frac{\partial (\rho Y_k)}{\partial t} + \nabla \cdot [\rho (V + V_k') Y_k] = \dot{\omega}_k \quad k = 1...N_S - 1 \tag{4}$$

where ρ is the density of the mixture, $V = (u, v)$ is the velocity vector, and P is the pressure. Y_k, V_k', and $\dot{\omega}_k$ are respectively the mass fraction, diffusion velocity, and production rate of the *k*-th species. The Arrhenius equation [33] is used to calculate ω_k and the mixture is modelled as the ideal gas. N_S is the total number of the species. The viscous stress is

$$\tau = \mu \left[\nabla V + (\nabla V)^T - \frac{2}{3} I (\nabla \cdot V) \right] \tag{5}$$

in which μ is the dynamic viscosity of the mixture and *I* is the unit tensor. We assume that the mixture is ideal gas and the equation of state is

$$P = \frac{\rho RT}{\overline{W}} \tag{6}$$

where *T* is the temperature, *R*=8.314 *J*/(mol•K) is the universal gas constant, and $\overline{W}$ is the mean molar weight of the mixture.

The heat flux *q* and total energy *E* in Eq. (3) are [33]:

$$q = -\lambda \nabla T + \rho \sum_{k=1}^{N_S} \left(Y_k h_k V_k' \right) \tag{7}$$

$$E = -\frac{P}{\rho} + \frac{V^2}{2} + \sum_{k=1}^{N_S} \left(Y_k h_k \right) \tag{8}$$

where λ is the thermal conductivity of the mixture, and h_k is the enthalpy of the *k*-th species.

The thermodynamic properties of each species are evaluated with JANAF polynomials [34]. The constant pressure specific heat capacity, C_P, is represented as a polynomial of temperature. Specifically, C_P is calculated by [34]

$$\frac{C_p}{R} = \sum_{n=0}^{6} a_n T^n \tag{9}$$

where a_n is the polynomial coefficient provided by the thermodynamic

Fig. 1. The computational model of the ODW/boundary layer interaction.

file.

The mixture-averaged transport model is used to calculate the transport properties. The Wilke formula is used to calculate the dynamic viscosity of the mixture [35]

$$\mu = \sum_{k=1}^{N_S} \frac{X_k \mu_k}{\sum_{j=1}^{N_S} X_j \Phi_{kj}} \tag{10}$$

where X_k is the mole fraction and μ_k is the dynamic viscosity coefficient of the k-th species. Φ_{kj} is the dimensionless partition function defined as [35]:

$$\Phi_{kj} = \frac{1}{\sqrt{8}} \left(1 + \frac{W_k}{W_j}\right)^{-\frac{1}{2}} \left[1 + \left(\frac{\mu_k}{\mu_j}\right)^{\frac{1}{2}} \left(\frac{W_j}{W_k}\right)^{\frac{1}{4}}\right]^2 \tag{11}$$

where W_k is the molecular weight of the k-th species.

The thermal conductivity of the mixture is obtained from the formula [36]:

$$\lambda = \frac{1}{2} \left(\sum_{k=1}^{N_S} X_k \lambda_k + \frac{1}{\sum_{k=1}^{N_S} \frac{X_k}{\lambda_k}} \right) \tag{12}$$

where λ_k is the thermal conductivity of the k-th species.

The thermal diffusion effect is neglected and the diffusion velocity, V'_k in Eq. (4), is calculated by [37]

$$V'_k = V'_{k,Y} + V'_{k,C} \tag{13}$$

where $V'_{k,Y}$ is the ordinary diffusion velocity, whose expression is [37]

$$V'_{k,Y} = -\frac{D_{km}}{X_k} \frac{\partial X_k}{\partial x_i} \tag{14}$$

where D_{km} is the mixture-averaged mass diffusion coefficient and Θ_k is the thermal diffusion ratio of the k-th species. The correction velocity, $V'_{k,C}$, is introduced to ensure the compatibility between the species mass conservation and the total mass conservation. It is determined according to the following requirement [37]

$$\sum_{k=1}^{N_S} \left(\rho Y_k V_k \right) = 0 \tag{15}$$

The compressible reacting flow solver, *detonationFoam* [38], developed based on OpenFOAM [39], is employed to solve the governing equations. Its capability in simulating gas-phase detonations has been thoroughly validated [40,41]. The second-order van-Leer scheme [42] is utilized for variable reconstruction and the pressure-corrected approximate Riemann solver, HLLC-P [43], is used to calculate the fluxes. For the diffusion terms, the second-order central difference scheme is adopted. A second-order backward difference scheme is utilized for time advance. The Courant number is used to calculate the time increment and fixed to 0.2. The stiff ordinary differential equation solver, *seulex*, which employs an extrapolation algorithm based on the linearly implicit Euler method with step size control and order selection, is used to handle the chemical reaction processes [44,45]. The grid sizes ranging from about 2.5 μm (near walls) to 18 μm (far away from walls) are used in the simulations. The grid independence test and numerical method validation are provided in the Supplementary Material.

3. Results and discussion

3.1. Inviscid ODW flow structures

The ODWs under inviscid conditions are simulated and presented in Fig. 2. Ma is fixed at 8. When $\theta_1 = 20°$, it is observed in Fig. 2(a) that an OSW is first induced by the wedge. The mixture is compressed by the OSW, leading to the formation of a reaction front (RF). Then the RF interacts with the OSW and evolves into an ODW. As the ODW impacts the upper wall, a reflected shock wave (RSW) is formed. When θ_1 is increased to 25°, the ODW has a Mach reflection on the upper wall and a normal detonation wave (NDW, it is also known as Mach stem, MS) can be observed. Besides, the ODW forms more closed to the wedge tip for the case $\theta_1 = 25°$ As θ_1 is further increased to 28° or 30°, the similar wave structures can be observed, and the MS height increases (see Fig. 2c-d).

In summary, when a slip wall is modeled, the ODW interacts directly
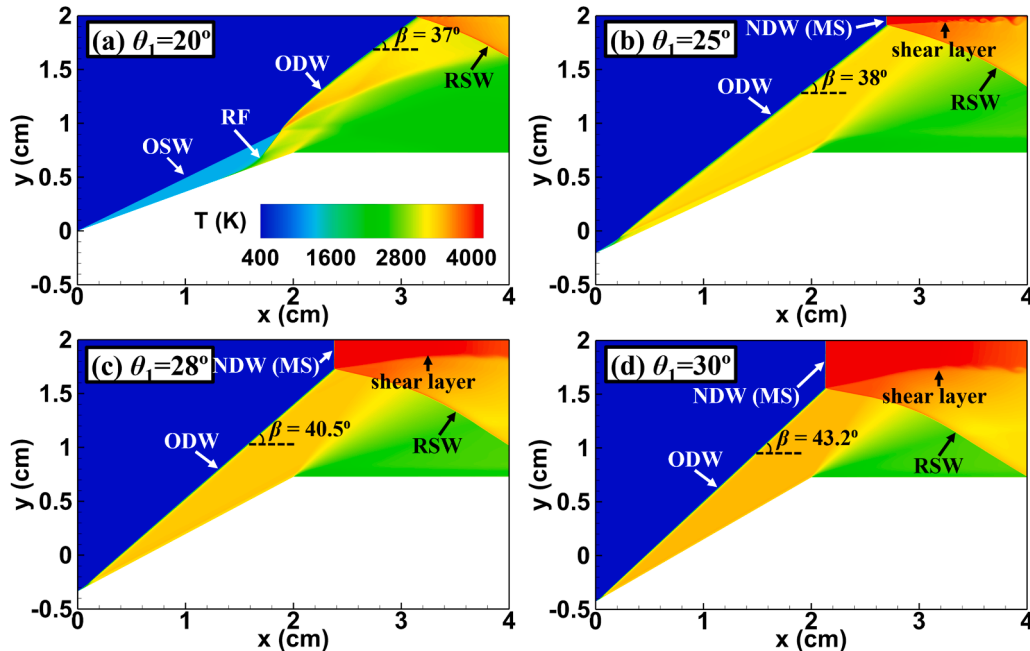

Fig. 2. Steady ODW temperature contours corresponding to the wedge angle $\theta_1 =$ (a) 20°, (b) 25°, (c) 28° and (d) 30° The inflow Mach number is fixed at 8 and viscosity is ignored.

with the upper slip wall, resulting in either regular or Mach reflections. The occurrence of these reflections depends significantly on the wedge angle; larger angles tend to favor Mach reflections. It should be noted that the wave system structure depicted in Fig. 2 is in a steady state, and the height of the Mach stem remains constant over time. But, if the Mach number decreases further, the Mach stem caused by the interaction between the ODW and the wall becomes unstable and propagates upstream [22].

3.2. Flow structures of ODW in a viscous channel

3.2.1. Role of the viscosity in ODW/wall interactions

In this section, the viscous effects are considered, i.e., the no-slip wall is modelled. We take the case of $Ma = 8$ and $\theta_1 = 20°$ as an example to illustrate how the viscosity influences the ODW structures. The steady ODW obtained under inviscid conditions from Fig. 2(a) is used as the initial field. The flow characteristics near the wedge and the upper wall under viscous conditions are depicted in Fig. 3 and Fig. 4, respectively.

From Fig. 3, it is seen that a boundary layer attaches the no-slip wall, and the reaction front (RF) forms on the wedge surface. Referring to the theory proposed by Teng et al. [8,46], the convergence of compression waves induced by the reaction front along the wedge surface is crucial for the transition of OSW to ODW. In the viscous case, the reaction front forms almost at the wedge tip, thereby accelerating the formation of compression waves and facilitating the OSW-ODW transition. Consequently, under viscous conditions, the ODW is located closer to the leading edge compared to the inviscid condition. Furthermore, if the OSW-ODW transition zone exhibits an abrupt transition with a reflected shock wave, the reflected shock will interact with the boundary layer on the wedge surface. It is likely to form a small recirculation zone [19].

When the no-slip wall is modelled, the ODW interacts with the boundary layer on the upper wall. The transient evolution of the flow structure near the upper wall are shown in Fig. 4. Fig. 4(a) shows that a high-pressure region is induced by ODW reflection on the upper wall at time $t = 0$. The pressure of the flow within the upstream boundary layer is lower than the pressure behind the RSW, forming an adverse pressure gradient to hinder the fluid from moving downstream. Hence the flow redirects, resulting in a separation zone, as illustrated in Fig. 4(b). As the fluid continually flows into the separation zone, the zone expands upstream (see Fig. 4b-d) until it reaches the leading edge of the upper wall, and then the morphology of the separation zone stabilizes. Fig. 4 (e-h) display the numerical schlieren contours during the development process of the separation zone. It is observed that a series of secondary oblique shock waves (SOSW) gradually propagate upstream, attaching to the separation zone. Details of the complex flow structures within the separation zone will be discussed subsequently.

To illustrate the fully developed ODW structures under viscous conditions, the temperature contour and numerical schlieren contour of ODW are shown in Fig. 5. Compared with the results obtained under inviscid conditions shown in Fig. 2(a), several difference can be observed. First, the wedge-induced ODW is positioned closer to the

wedge tip. Second, the interaction between the ODW and the upper wall boundary layer induces a large separation structure consisting of oblique shock wave (OSW#2), reaction front (RF#2), secondary oblique shock waves (SOSWs) and the separation zone, as signed in Fig. 5.

To show the detailed flow structures within the separation zone from Fig. 5, the streamline, vorticity, velocity and temperature distributions near the separation zone on the upper wall are plotted in Fig. 6. The streamlines in Fig. 6(a) reveal that there are a series of separation bubbles in separation zone. The vorticity within separation zone, as depicted in Fig. 6(b), is significantly higher than that in the surrounding regions. Fig. 6(c) illustrates that the flow velocity within separation zone is low, allowing the mixture to stay for a sufficient time and auto-ignite. Since the combustion products are confined within separation zone, the temperature in separation zone reaches approximately 3800 K, as illustrated in Fig. 6(d). Besides, the separation zone acts as an aerodynamic wedge to impede the high-speed incoming mixture. An oblique shock wave (OSW#2 in Fig. 6d) is induced when the inflow impacts the aerodynamic wedge. OSW#2 compresses the incoming mixture, causing its temperature rise to about 1000 K. Then the mixture auto-ignites, leading to the formation of a slender reaction front (RF#2 in Fig. 6d) between the separation zone and OSW#2. Note that the flow velocity near RF#2 is substantially higher than that within the separation zone (see Fig. 6c). Hence, the reaction products between OSW#2 and separation zone swiftly flow downstream, preventing heat accumulation and resulting in a lower temperature than that observed within the separation zone.

3.2.2. Effects of wedge angle on ODW flow structures

Next, while maintaining the inflow Mach number as 8, we increase the wedge angle to 25° and the simulation results are shown in Fig. 7. Compared with the results in Fig. 5, the main flow structures in Fig. 7 have no significant difference. There is also an oblique detonation wave (signed with ODW#1 in Fig. 7) induced by the wedge and a separation zone near the upper wall. However, when $\theta_1 = 25°$, the separation zone induces a new oblique detonation wave (signed with ODW#2 in Fig. 7) near the upper wall instead of the OSW-RF-separation zone structure observed in Figs. 5 and 6.

To further illustrate that the separation zone directly induces an oblique detonation wave for case $\theta_1 = 25°$, we extract the pressure and temperature distributions along line $y = 1.5$ cm for cases of $\theta_1 = 20°$ and $\theta_1 = 25°$ For the case of $\theta_1 = 20°$ shown in Fig. 8(a), the oblique shock wave (OSW#2) compresses the mixture, increasing the pressure from 1 atm to 4 atm at $x \approx 1.45$ cm. Concurrently, the mixture temperature rises to approximately 700 K. At $x \approx 2.20$ cm, the temperature sharply increases to around 2200 K due to the autoignition of the mixture. These results indicate that the shock wave and the reaction front are sufficiently separated and in a decoupled state. However, when $\theta_1 = 25°$, as shown in Fig. 8(b), at $x \approx 0.80$ cm, the pressure increases to 18 atm and the mixture temperature rises from 400 K to approximately 2700 K, indicating that the mixture auto-ignites at the shock wave location. This results in the formation of a detonation wave, where the shock wave and
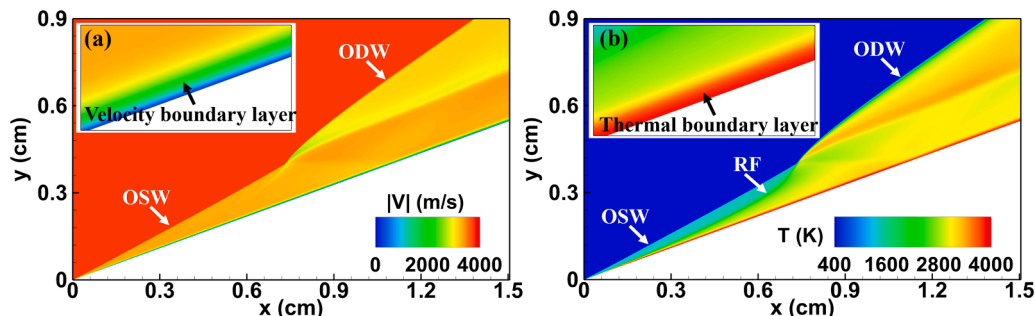

Fig. 3. (a) Velocity and (b) temperature distributions near the wedge wall under viscous condition. $Ma = 8$ and $\theta_1 = 20°$
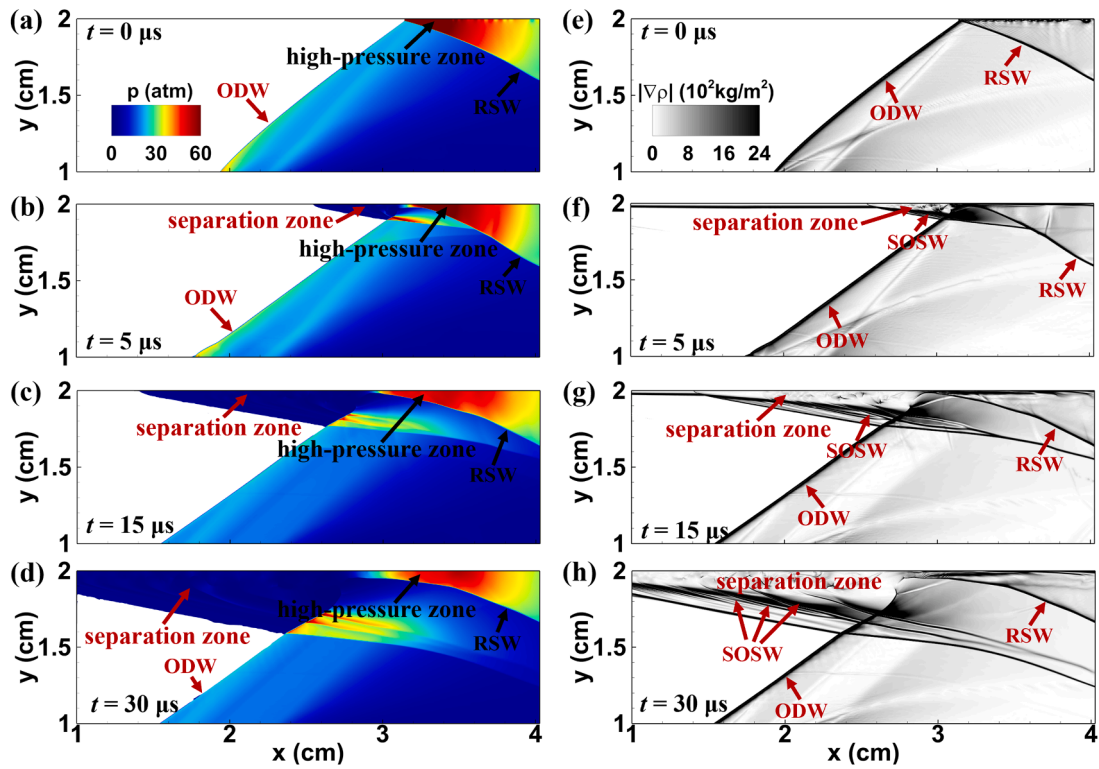
Fig. 4. Temporal (a-d) pressure and (e-h) numerical schlieren contours near the upper wall to show how the separation zone develops. $Ma = 8$ and $\theta_1 = 20°$
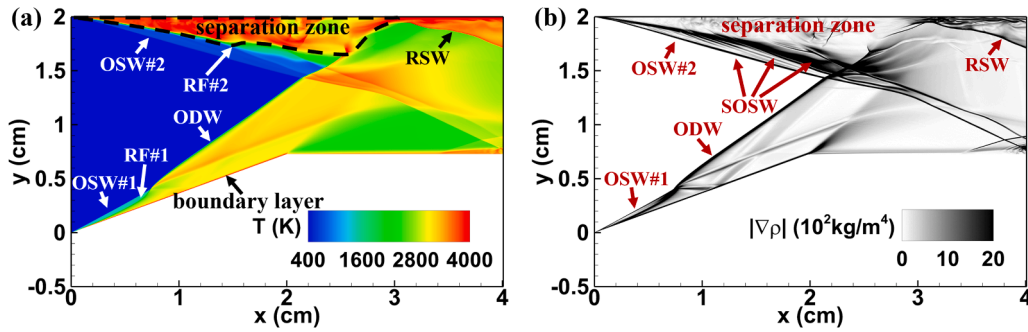

Fig. 5. Steady oblique detonation wave structure predicted under viscous condition. (a) Temperature contour; (b) Numerical schlieren contour. $Ma = 8$ and $\theta_1 = 20°$
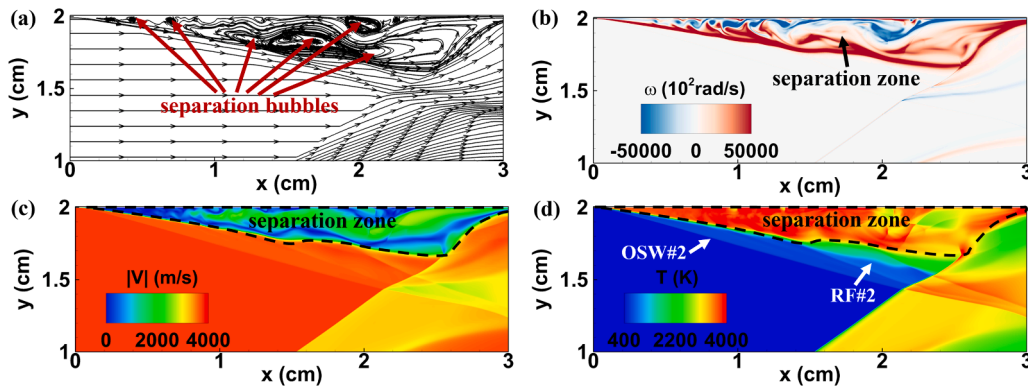

Fig. 6. Inserts of (a) streamline, (b) vorticity, (c) absolute velocity and (d) temperature distributions near the separation zone on the upper wall. $Ma = 8$ and $\theta_1 = 20°$

the reaction front are coupled.

When the wedge angle is further increased to 30°, the temperature contour and numerical schlieren contours are recorded in Fig. 9. Similar

to the results of $\theta_1 = 25°$ shown in Fig. 7, the wedge-induced ODW (signed as ODW#1 in Fig. 9) interacts with the upper wall boundary layer, leading to the formation of a separation zone and an ODW (signed
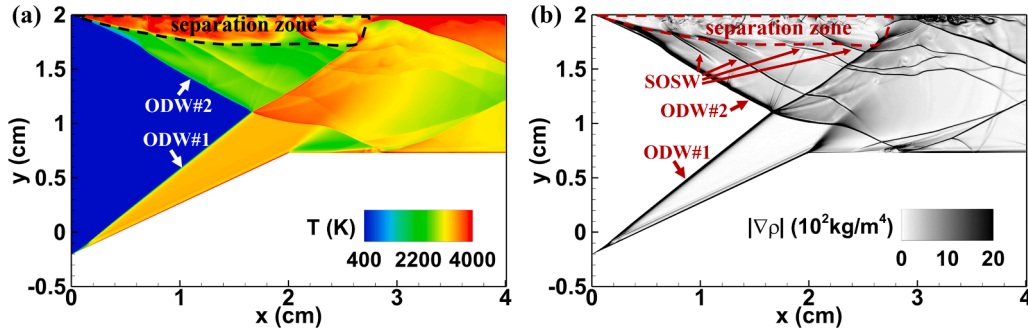
Fig. 7. Oblique detonation wave structure predicted under viscous conditions. (a) Temperature contour; (b) Numerical schlieren contour. $Ma = 8$ and $\theta_1 = 25°$
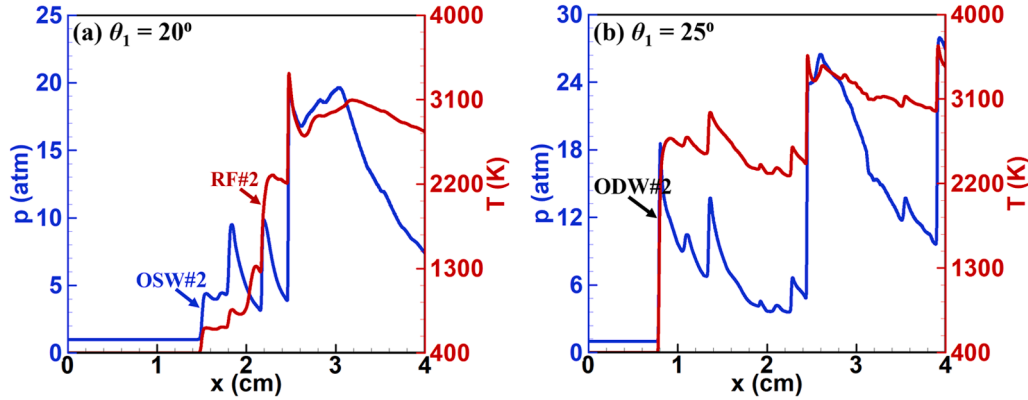

Fig. 8. Pressure and temperature distributions along the line $y = 1.5$ cm of the oblique detonation wave acquired under conditions of $\theta_1 =$ (a) 20° and (b) 25° The inflow Mach number is fixed to 8.
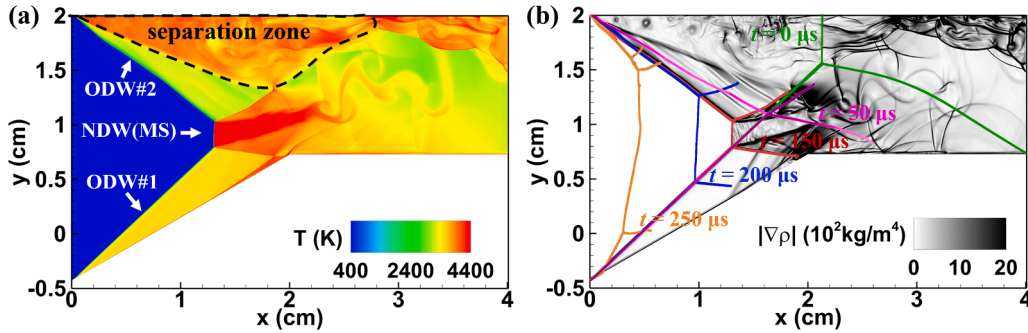

Fig. 9. Oblique detonation wave structure: (a) Temperature contour, (b) numerical schlieren contour at $t = 150$ μs and the temporal wave front positions of the oblique detonation wave structure under viscous condition. $Ma = 8$ and $\theta_1 = 30°$

as ODW#2 in Fig. 9). The difference is that ODW#1 and ODW#2 for case of $\theta_1 = 30°$ are connected by a NDW, rather than the direct contact as observed for case of $\theta_1 = 25°$ in Fig. 7. It is emphasized that the flow structures shown in Fig. 9(a) are unsteady and we present the wave fronts at different instants in Fig. 9(b). The results show that the NDW continuously moves upstream and eventually engulfs the entire ODWs, leading to the failed detonation.

The influence of viscosity on ODW structures is primarily manifested in the formation of the separation zone, which is caused by the interaction between the wedge-induced ODW and the boundary layer on the upper wall. This interaction results from the significant adverse pressure gradient caused by the reflection of the detonation wave. The detailed flow structures vary relative to the wedge angle. Specifically, when the wedge angle is relatively small ($\theta_1 = 20°$), the separation zone induces an OSW that interacts directly with the wedge-induced ODW. As θ_1 increases to 25°, the separation zone on the upper wall induces an ODW

that also connects directly to the wedge-induced ODW. When θ_1 is further increased to 30°, the separation-induced ODW and the wedge-induced ODW connect through a Mach stem. This Mach stem continuously moves upstream, ultimately leading to detonation failure.

3.2.3. Effects of wall temperature on flow separation structures

This section aims to illustrate the effects of wall temperature on the flow separation structure based on Fig. 7 ($Ma = 8$, $\theta_1 = 25°$). The adiabatic wall condition is modified to an isothermal wall assumption, and the ODW structures are numerically simulated for different wall temperatures (T_W). Fig. 10 shows the ODW temperature contours for wall temperatures of 2000 K, 1200 K, and 400 K, respectively. When the T_W is 2000 K, the leading edge-induced separation zone first induces an oblique shock wave (OSW#2), which gradually transitions into an oblique detonation wave (ODW#2). Compared to results of adiabatic wall in Fig. 7, the transition distance from OSW#2 to ODW#2 is longer
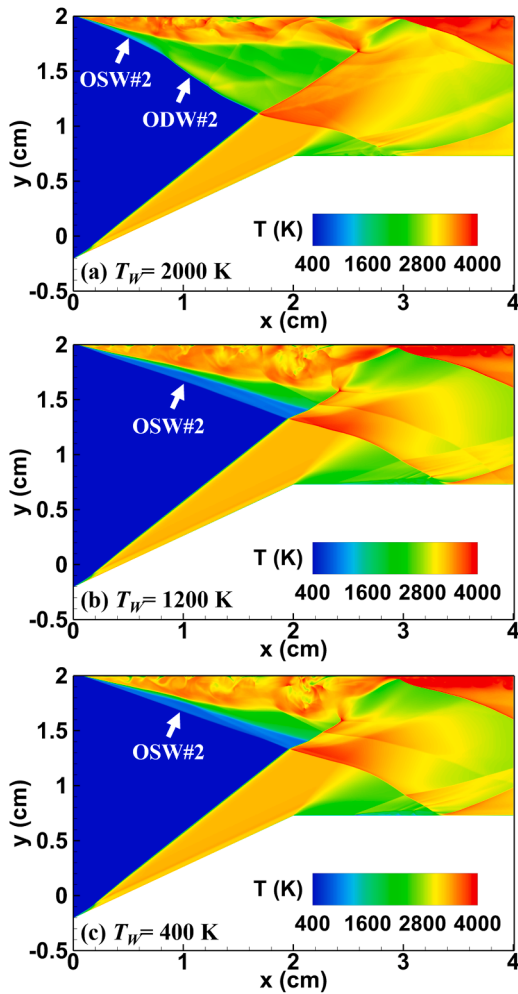
Fig. 11. Pressure profiles along the line $y = 1.9$ cm for different wall temperature conditions. $Ma = 8$ and $\theta_1 = 25°$

Fig. 10. Temperature contours of the steady oblique detonation wave predicted by adopting different wall temperature models for case of $Ma = 8$ and $\theta_1 = 25°$ (a) $T_W = 2000$ K; (b) $T_W = 1200$ K; (c) $T_W = 400$ K.

in Fig. 10(a). For hypersonic reactive flows, the viscous wall not only decelerates the fluid but also triggers intense chemical reactions. The wall temperature of an adiabatic wall depends on the local flow conditions and typically exceeds 3000 K under adiabatic assumptions for the Mach number of 8. The heating effect of the wall promotes the transition from OSW#2 to ODW#2.

To validate the aforementioned claims, we reduce the wall temperature to 1200 K and 400 K under the isothermal wall assumption and present the results in Fig. 10(b) and (c). From these figures, it can be observed that the separation zone only induces the OSW#2. This further demonstrates that high wall temperatures facilitate the transition from oblique shock to oblique detonation. For isothermal walls, when the wall temperature is lower than the fluid temperature within the separation zone, it exerts a cooling effect on the separation zone, reducing its angle and weakening the intensity of OSW#2. Fig. 11 shows the pressure distribution along $y = 1.9$ cm under different wall conditions. It can be seen that the strength of the separation-induced OSW#2 decreases with decreasing wall temperature, confirming the above analysis. Therefore, under adiabatic conditions, the separation zone induced by the leading edge can directly induce the ODW#2, while the transition distance from OSW#2 to ODW#2 increases under the isothermal wall condition of 2000 K. In contrast, When T_W equals to 1200 K or 400 K, only the OSW#2 is induced. Additionally, it is found that the separation zones in Fig. 10(b) and (c) are triangular, whereas the separation zone in Fig. 10(a) resembles an inverted trapezoid. This is primarily due to the presence
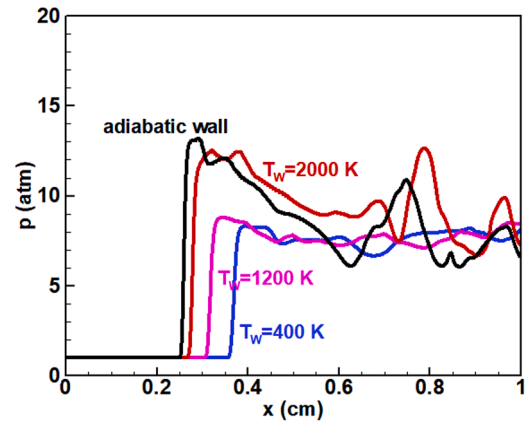
of ODW#2, which exerts higher post-wave pressure, compressing the separation zone upward. Similar phenomena can be observed in Fig. 7.

The simulated results indicate that wall temperature has a quantitative effect on the wave system of the separation flow, even altering the wave system's morphology. Similar to parameters such as wedge angle, wall temperature can influence the local flow characteristics of the detonation wave system. However, for the three basic flow wave systems identified in this study (namely, separation shock-dominated systems, separation detonation-dominated systems, and unstable Mach stem-dominated systems), wall temperature does not fundamentally alter their nature. Lowering the wall temperature merely delays or suppresses the transition from OSW#2 to ODW#2, which essentially results from the reduced strength of OSW#2. Therefore, increasing the wedge angle can further enhance the strength of OSW#2, promoting the emergence of ODW#2. However, it must be acknowledged that the influence of wall temperature on detonation wave systems is complex. In practical engineering applications, the wall is neither perfectly adiabatic nor isothermal; it is likely to exhibit a non-uniform temperature spatial distribution. This study focuses more on idealized models to provide macroscopic flow characteristics of detonation wave systems.

3.3. Discussion on flow structure formations

3.3.1. Analysis on wave system patterns

Considering the interaction between the ODW and the viscous wall, there are three typical flow characteristics of detonation wave in confined spaces: separation shock-dominated systems, separation detonation-dominated systems, and unstable Mach stem-dominated systems. Corresponding diagrams are shown in Fig. 12. The first two are quasi-steady wave systems, where the detonation wave does not continuously propagate upstream, while the latter experiences flow choking, rendering the normal detonation wave unstable. Although factors such as wedge angle, Mach number, and wall temperature influence the type of flow wave system, the primary characteristics can be categorized into these three types. The main differences among these flow wave systems lies in whether the separation zone induced by the leading edge can induce an ODW and whether the ODW undergoes a Mach reflection.

To explain why the separation zone can induce an ODW, Fig. 13 depicts the pressure field, density gradient, and vorticity distribution near the separation zone under different wedge angles. The figure shows that the leading edge of the separation zone induces an OSW, and as the angle of the recirculation zone increases, the angle and pressure of the OSW/ODW also increase. Therefore, the separation zone acts as an aerodynamic wedge. Previous study has shown that an increase in the aerodynamic wedge angle enhances the OSW [47], which naturally promotes the autoignition of the reactants behind the wave, leading to
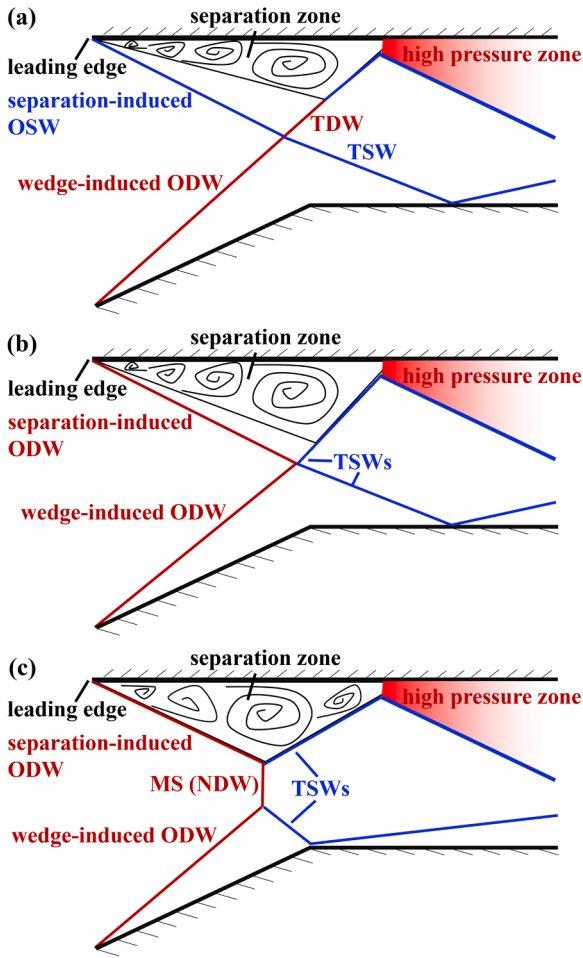
(a)

(b)

(c)

Fig. 12. Three types of typical detonation wave system diagrams: (a) separation shock-dominated wave systems, (b) separation detonation-dominated wave systems, and (c) unstable Mach stem-dominated wave systems.

the formation of a detonation wave.

However, why the angle of the recirculation zone increases is another interesting phenomenon. It is generally believed that the presence of an adverse pressure gradient causes the fluid to decelerate, even leading to a change in flow direction and resulting in flow separation. The greater the adverse pressure gradient, the more severe the flow separation, which is manifested by the separation point moving

continuously upstream. In the context of this study's physical model, the flow separation is induced by the leading edge, and the length of the upper wall is limited (see Fig. 1), restricting the continuous upstream movement of the separation point. As the wedge angle continues to increase and ODW#1 strengthens, the pressure at the tail of the recirculation zone continuously increases. The recirculation zone cannot move along the flow direction and thus expands longitudinally, leading to an increase in the angle of the recirculation zone. A similar phenomenon can be observed in literature related to leading edge-induced separation [47], where an increase in wedge angle, with a fixed incoming Mach number, results in an increased longitudinal size of the separation zone.

The interaction types between OSW#2/ODW#2 and ODW#1 can be explained using shock wave/detonation polar curves. It should be noted that the flow wave systems in this study are mostly quasi-steady or unsteady. The shock wave/detonation wave polar curves are more applicable to planar and steady-state wave systems. Therefore, we use the polar curve theory to qualitatively explain the formation of regular and Mach reflection, without intending to precisely predict the flow parameters. Fig. 14 shows the pressure contours and schematic diagrams of the wave systems near the OSW#2/ODW#2 and ODW#1 interaction zones for wedge angles of 20° and 30°, respectively. The black lines with arrows indicate streamlines.

For the case of $\theta_1 = 20°$ and $Ma = 8$, the separation-induced OSW (sign with OSW#2) directly interacts with the wedge-induced ODW (ODW#1), a regular reflection occurs. The transmitted wave system consists of a transmitted shock wave (TSW) and a transmitted detonation wave (TDW). Due to the difference in the intensity of the waves, the gas stream behind the interaction point experiences a slight deflection. In Fig. 14(b), we plot the polar curves for OSW#2, ODW#1, TSW, and TDW. When the mixture transitions from region II or III to region IV, the pressures behind TSW and TDW are equal near the interaction point, based on the principle of pressure matching. This corresponds to the intersection point on the TSW and TDW polar curves in Fig. 14(b). Importantly, the weak solution branches of TSW and TDW intersect below the strong solution branches of ODW#1 and OSW#2. Therefore, the interaction type between ODW#1 and OSW#2 should be regular reflection.

The results for the case with $\theta_1 = 30°$ and $Ma = 8$ are shown in Fig. 14 (c). ODW#2 and ODW#1 are no longer directly connected; they are linked through a vertical Mach stem. Unlike regular reflection, the wave system in Fig. 14(c) is typically referred to as Mach reflection and there are two interaction points above and below the Mach stem. The notable differences in the streamline angles between regions V and IV can be observed, indicating that the flow state in region VI and the intensity of the Mach stem are not uniform.

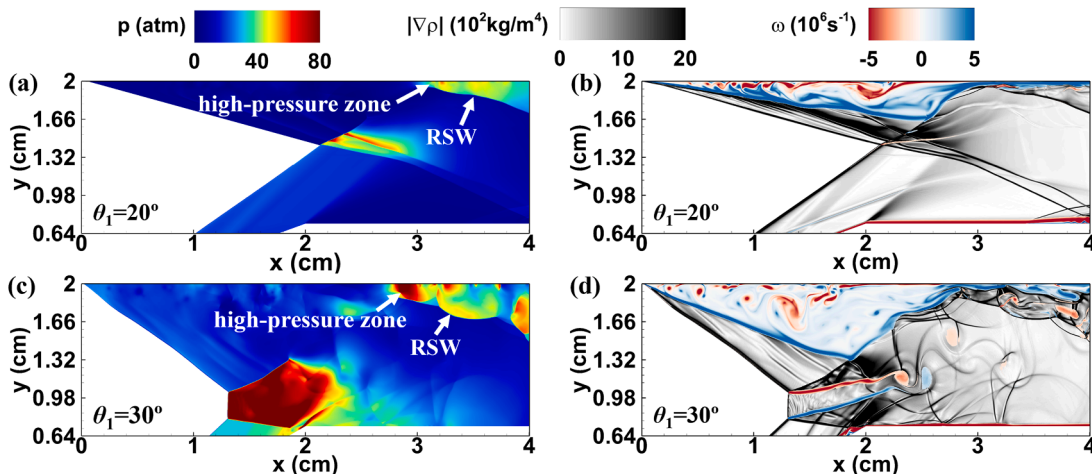In the p-θ polar curve shown in Fig. 14(d), there is an intersection

Fig. 13. Pressure (a, c), density gradient (b, d), and vorticity (b, d) distribution near the separation zone. $Ma = 8$, $\theta_1 = 20°$ (a, b) and 30° (c, d).
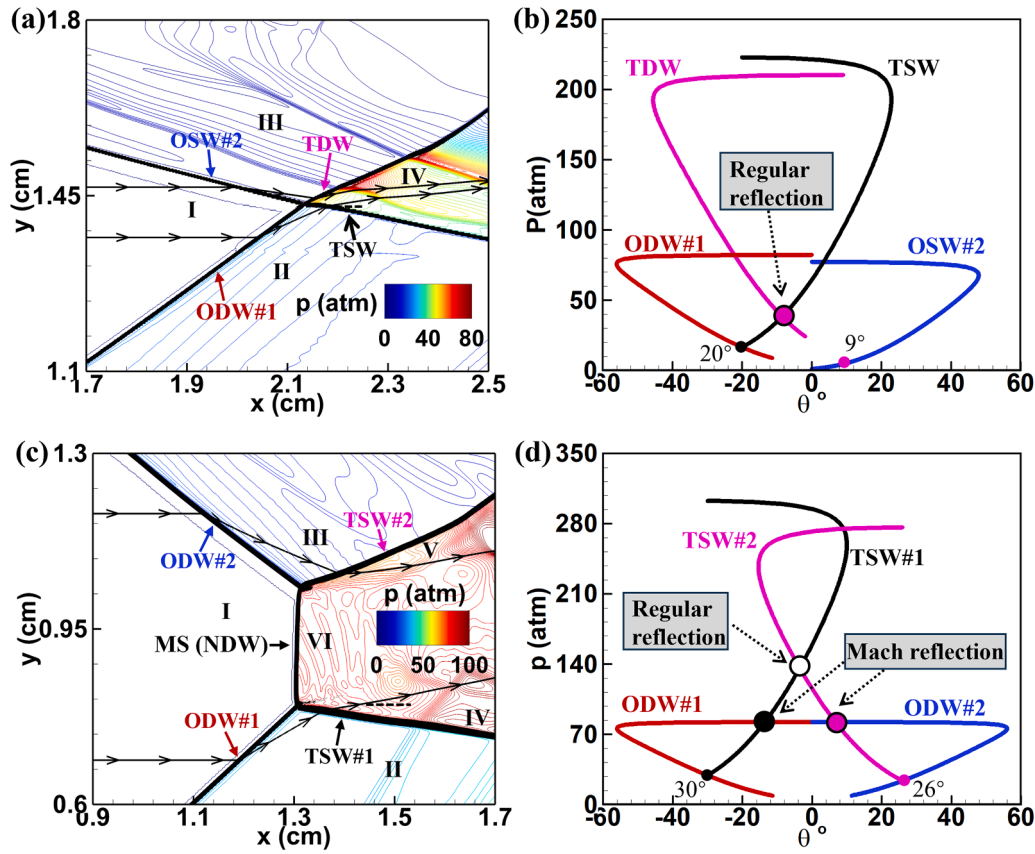
Fig. 14. Local pressure isopleths (a) and p-θ polar curves of the detonation/shock waves (b) for the case of $\theta_1 = 20°$ and $Ma = 8$; local pressure isopleths (c) and p-θ polar curves of the detonation/shock waves (d) for the case of $\theta_1 = 30°$ and $Ma = 8$.

point between the two TSW curves, which corresponds to the regular flow state. Additionally, the intersection between the weak solution branch of TSW and the strong solution branch of ODW represents the Mach reflection flow state. According to the traditional shock polar curve theory [48], the flow conditions at this point can exist in both regular and Mach flow states, indicating they are in a dual-solution domain. The specific form of shock reflection within the dual-solution domain depends on initial conditions and local flow field. In the context of this study, when the wedge angle is 30°, flow choking occurs. The regular flow presented by the intersection point between the two TSW curves in Fig. 14(d) mainly occurs in the early stage of the unsteady wave system (see Fig. 9b). Over time, the interaction type between the OSW#2/ODW#2 and the ODW#1 gradually changes from regular reflection to Mach reflection (see Fig. 14c).

3.3.2. Relationship between inviscid and viscous flows

In inviscid flow, the interaction between the ODW and the upper wall primarily results in two types of wave systems: regular reflection and Mach reflection (which differ from the interaction between OSW#2 and ODW#1 discussed in Section 3.3.1). In contrast, in viscous flow, there are three typical types of wave systems, which primarily depend on parameters such as wedge angle. To explore the relationship between inviscid and viscous flow wave systems, we expand the parameter range to simulate the ODW structures for inflow Mach numbers from 7 to 8.5 and wedge angles from 20° to 30° (including both inviscid and viscous cases). We name the three types of detonation wave systems obtained in viscous flow as follows: Mode #1, where the separation zone on the upper wall induces an OSW; Mode #2, where the separation zone induces an ODW; and Mode #3, where the wedge-induced ODW and the separation-induced OSW/ODW interact, resulting in flow choking.

It is important to note that, under the inflow conditions used in this

study, the height of the Mach stem in inviscid flow is a constant value. Therefore, we measured the height of the Mach stem in the inviscid cases and defined the dimensionless parameter η as the ratio of this height to the height of the combustion chamber entrance. For regular reflection, the height of the Mach stem equals zero, i.e., $\eta = 0$.

Using Mach number as the horizontal axis and the dimensionless parameter η as the vertical axis, we plotted the distribution of viscous flow wave system types under different wedge angles, as shown in Fig. 15. The above discussion illustrates that the combustion mode transitions from Mode #1 to Mode #2, and subsequently to Mode #3, as the wedge angle increases. Fig. 15 indicates that at a fixed wedge angle
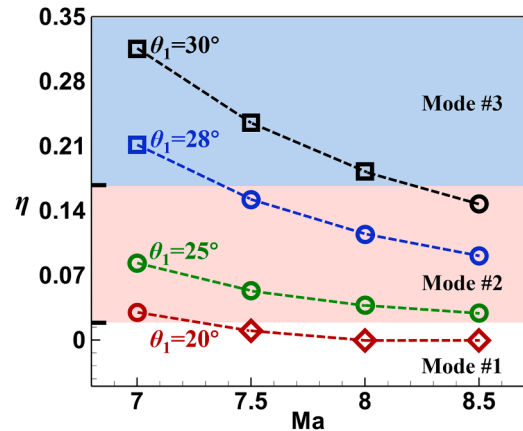

Fig. 15. Combustion modes and the η values corresponding to different inflow Mach numbers ($Ma = 7$, 7.5, 8 and 8.5) and different wedge angles ($\theta_1 = 20°$, 25°, 28° and 30°). ◇: Mode #1; ○: Mode #2; □: Mode #3.

of 20°, decreasing the Mach number from 7.5 to 7 shifts the combustion mode from Mode #1 to Mode #2. Similarly, at a wedge angle of 28°, decreasing the Mach number from 7.5 to 7 changes the combustion mode from Mode #2 to Mode #3. Thus, when the wedge angle is fixed, increasing inflow Mach number results in a transition from Mode #3 to Mode #2, and finally to Mode #1.

More importantly, using η (obtained from inviscid flow) effectively distinguishes between the different flow modes of viscous ODW. This shows a correlation between viscous flow and inviscid wave systems, as both inviscid Mach stems and viscous recirculation zones can obstruct the high-speed flows. For cases conducted under viscous conditions, as the wedge angle increases, the angle of ODW#1 increases. This causes the longitudinal size of the recirculation zone to rapidly expand, significantly reducing the actual flow area of the channel. The recirculation zone obstructs the high-speed flow, forcing the airflow at the left entrance to deflect to adapt to the actual flow area. This deflection is primarily achieved through the OSW/ODW induced by the recirculation zone.

In the inviscid scenario, the presence of a Mach stem reduces the supersonic flow, leading to a large subsonic region within the channel. The larger the wedge angle, the greater the area of the subsonic region. The appearance of a subsonic region behind the Mach stem also limits the channel's flow capacity and can even cause flow choking. This is similar to the obstructive effect of the recirculation zone on high-speed flows. Therefore, although the dimensionless parameter η is defined under inviscid conditions, its physical essence (acting as a flow obstruction) is consistent with that of the recirculation zone. This provides a simpler criterion for determining the stability of detonation wave systems under viscous conditions: by establishing a mapping relationship between the instability characteristics of inviscid and viscous flow fields, we can use the results of rapid inviscid numerical simulations to determine the instability boundary of viscous ODWs.

4. Conclusions

This study numerically examines the wedge-induced ODW structures for stoichiometric H_2/air mixtures with detailed chemistry in limited spaces. The investigation spans a range of incoming Mach numbers from 7 to 8.5 and wedge angles from 20° to 30° The focus is on evaluating the effect of viscosity on the morphology of ODW, particularly the interaction patterns between the ODW and the boundary layer.

Results show that the viscosity has a dual effect on flow structures. Firstly, within the boundary layer, the mixture auto-ignites, facilitating the transition from OSW to ODW. Under viscous conditions, the wedge-induced ODW is closer to the wedge tip compared to inviscid cases. Secondly, the wedge-induced ODW interacts with the boundary layer on the upper wall, leading to a significant separation zone. The separation zone acts as an aerodynamic wedge, inducing the OSW/ODW in the supersonic flow. The interaction between the wedge-induced ODW and the separation-induced OSW/ODW results in two different wave reflections: regular or Mach reflection. Based on the interaction characteristics of the OSW/ODW induced by the separation zone, three typical flow wave systems, namely separation shock-dominated wave systems, separation detonation-dominated wave systems, and unstable Mach stem-dominated wave systems, can be observed for different wedge angles, Mach numbers, and wall conditions.

The influence of external factors such as wedge angles, Mach numbers, and wall conditions can be summarized by their effects on the angle of the separation zone. When the angle of the separation zone is minimal, only an OSW-RF structure forms near the upper wall. As the separation zone angle increases, the OSW induced by the separation zone gradually transitions into an ODW. Simultaneously, the actual flow area within the combustion chamber decreases, potentially leading to flow choking. Furthermore, by using the dimensionless parameter η (defined as the ratio of the inviscid Mach stem height to the combustion chamber entrance height), we attempt to establish a correlation between

the characteristics of inviscid and viscous flow wave systems. We find that η effectively distinguishes between the three typical wave systems of viscous flow. This is primarily because both the inviscid Mach stem and the viscous recirculation zone act as flow obstructions.

The findings of this study highlight the significant influence of boundary layer/ODW interactions on flow structures within confined combustion chambers. Therefore, numerical simulations of ODWs within confined spaces should account for boundary layer effects. This study is limited to two-dimensional simulations; and it is recognized that the stability of the separation bubbles observed here may differ in three-dimensional simulations. Therefore, conducting comprehensive three-dimensional simulations and focusing on the interaction between ODWs and turbulent boundary layers, would be attractive in future work.

Novelty and significance statement

The innovation of this work lies in the comprehensive assessment of the viscosity effects on the structure of oblique detonation waves within a confined combustion chamber configuration. The findings reveal that the interactions between oblique detonation waves and the boundary layer significantly influence flow characteristics and combustion regimes, with underlying mechanisms elucidated. Besides, the influence of Mach numbers, wedge angles and wall temperatures on flow structures are evaluated.

The significance of this work is that unlike the regular or Mach reflection observed under inviscid conditions, considering viscosity leads to a direct interaction between oblique detonation waves and the wall boundary layer. This interaction induces flow separation and the formation of corresponding separation-induced oblique shock/detonation waves. Consequently, the study enhances our comprehension of the dynamics and mechanisms governing oblique detonation wave-boundary layer interactions, offering crucial insights for the design of oblique detonation engines.

CRediT authorship contribution statement

Jie Sun: Writing – review & editing, Writing – original draft, Validation, Software, Methodology, Investigation. **Pengfei Yang:** Writing – review & editing, Writing – original draft, Supervision, Investigation, Funding acquisition. **Zheng Chen:** Writing – review & editing, Writing – original draft, Supervision.

Declaration of competing interest

The authors declare that they have no known competing financial interests or personal relationships that could have appeared to influence the work reported in this paper.

Acknowledgment

Supplementary materials

Supplementary material associated with this article can be found, in the online version, at doi:10.1016/j.combustflame.2024.113832.

References

[1] J.H.S. Lee, The Detonation Phenomenon, Cambridge University Press, 2008.
[2] K. Kailasanath, Review of propulsion applications of detonation waves, AIAA J. 38 (2000) 1698–1708.
[3] P. Wolański, Detonative propulsion, Proc. Combust. Inst. 34 (2013) 125–158.

[4] G.D. Roy, S.M. Frolov, A.A. Borisov, D.W. Netzer, Pulse detonation propulsion: challenges, current status, and future perspective, Prog. Energy Combust. Sci. 30 (2004) 545–672.

[5] Q. Xie, Z. Ji, H. Wen, Z. Ren, P. Wolanski, B. Wang, Review on the rotating detonation engine and it's typical problems, Trans. Aerosp. Res. 2020 (2020) 107–163.

[6] M. Shikun, Z. Jin, L. Yu, L. Shijie, L. Zhiyong, Review of studies on oblique detonation waves in supersonic flows, J. Exp. Fluid Mech. 33 (2019) 41–53.

[7] Z. Jiang, Standing oblique detonation for hypersonic propulsion: a review, Prog. Aerosp. Sci. 143 (2023) 100955.

[8] H. Teng, C. Tian, Y. Zhang, L. Zhou, H.D. Ng, Morphology of oblique detonation waves in a stoichiometric hydrogen–air mixture, J. Fluid. Mech. 913 (2021) A1.

[9] L.F.F.D. Silva, B. Deshaies, Stabilization of an oblique detonation wave by a wedge: a parametric numerical study, Combust. Flame 121 (2000) 152–166.

[10] J. Verreault, A.J. Higgins, Initiation of detonation by conical projectiles, Proc. Combust. Inst. 33 (2011) 2311–2318.

[11] A.-F. Wang, W. Zhao, Z.-L. Jiang, The criterion of the existence or inexistence of transverse shock wave at wedge supported oblique detonation wave, Acta Mech. Sin. 27 (2011) 611–619.

[12] P. Yang, H. Teng, Z. Jiang, H.D. Ng, Effects of inflow Mach number on oblique detonation initiation with a two-step induction-reaction kinetic model, Combust. Flame 193 (2018) 246–256.

[13] W. Dan, W. Jianping, Influences of viscosity and thermal conductivity on detonation waves, Chin. J. Appl. Mech. 29 (2012) 630–635.

[14] K. Mazaheri, Y. Mahmoudi, M.I. Radulescu, Diffusion and hydrodynamic instabilities in gaseous detonations, Combust. Flame 159 (2012) 2138–2154.

[15] H.H. Teng, Z.L. Jiang, On the transition pattern of the oblique detonation structure, J. Fluid. Mech. 713 (2012) 659–669.

[16] C. Li, K. Kailasanath, E. Oran, Effects of boundary layers on oblique-detonation structures, in: Proceedings of the 31st Aerospace Sciences Meeting, Reno, NV, 1993.

[17] C. Li, K. Kailasanath, E.S. Oran, Detonation structures behind oblique shocks, Phys. Fluids 6 (1994) 1600–1611.

[18] Y. Fang, Z. Zhang, Z. Hu, Effects of boundary layer on wedge-induced oblique detonation structures in hydrogen-air mixtures, Int. J. Hydrogen Energy 44 (2019) 23429–23435.

[19] S. Desai, Y. Tao, R. Sivaramakrishnan, J.H. Chen, Effects of non-thermal termolecular reactions on wedge-induced oblique detonation waves, Combust. Flame 257 (2023) 112681.

[20] L. Yang, L. Yue, D. Yu, Z. Chen, Numerical study on wave configuration of wedge-induced oblique detonation wave: reactive boundary layer effect, Phys. Fluids 34 (2022) 116103.

[21] C.L. Bachman, G.B. Goodwin, Ignition criteria and the effect of boundary layers on wedge-stabilized oblique detonation waves, Combust. Flame 223 (2021) 271–283.

[22] K. Wang, H. Teng, P. Yang, H.D. Ng, Numerical investigation of flow structures resulting from the interaction between an oblique detonation wave and an upper expansion corner, J. Fluid. Mech. 903 (2020) A28.

[23] K. Wang, Z. Zhang, P. Yang, H. Teng, Numerical study on reflection of an oblique detonation wave on an outward turning wall, Phys. Fluids 32 (2020) 046101.

[24] Z. Zhang, Y. Liu, C. Wen, Mechanisms of the destabilized Mach reflection of inviscid oblique detonation waves before an expansion corner, J. Fluid. Mech. 940 (2022) A29.

[25] Y. Wang, J. Liang, X. Cai, Y. Mahmoudi, Generation mechanism of a new type of unburnt gas pocket and its influences on the detonation-wave/boundary-layer interaction, Phys. Fluids 34 (2022) 041704.

[26] X. Cai, J. Liang, R. Deiterding, Y. Mahmoudi, M. Sun, Experimental and numerical investigations on propagating modes of detonations: detonation wave/boundary layer interaction, Combust. Flame 190 (2018) 201–215.

[27] V. Daru, C. Tenaud, Numerical simulation of the viscous shock tube problem by using a high resolution monotonicity-preserving scheme, Comput. Fluids. 38 (2009) 664–676.

[28] C. Huang, Y. Wang, R. Deiterding, D. Yu, Z. Chen, Numerical studies on weak and strong ignition induced by reflected shock and boundary layer interaction, Acta Mech. Sin. 38 (2022) 121466.

[29] S. Chen, Q. Sun, I. Klioutchnikov, H. Olivier, Numerical study of chemically reacting flow in a shock tube using a high-order point-implicit scheme, Comput. Fluids 184 (2019) 107–118.

[30] W. Chen, J. Liang, X. Cai, Z. Lin, Detonation interaction with boundary layer in supersonic combustible mixture, in: Proceedings of the 21st AIAA International Space Planes and Hypersonics Technologies Conference, Xiamen, China, 2017. AIAA-Paper 2017-2234.

[31] W. Chen, J. Liang, X. Cai, Z. Lin, The initiation and propagation of detonation in supersonic combustible flow with boundary layer, Int. J. Hydrogen Energy 43 (2018) 12460–12472.

[32] M.P. Burke, M. Chaos, Y. Ju, F.L. Dryer, S.J. Klippenstein, Comprehensive H_2/O_2 kinetic model for high-pressure combustion, Int. J. Chem. Kinet. 44 (2012) 444–474.

[33] T. Poinsot, D. Veynante, Theoretical and Numerical Combustion, R.T. Edwards, Inc., 2005.

[34] T.K. Risch, Curve Fits of the NIST-JANNAF Thermochemical Tables, 4th Edition, U. S. National Bureau of Standards, 2021 ed.

[35] C.R. Wilke, A viscosity equation for gas mixtures, J. Chem. Phys. 18 (1950) 517–519.

[36] P.K.T.S. Mathur, S.C. Saxena, Thermal conductivity of binary, ternary and quaternary mixtures of rare gases, Mol. Phys. 12 (1967) 569–579.

[37] F.M.R.R.J. Kee, J.A. Miller, M.E. Coltrin, J.F. Grcar, E. Meeks, H.K. Moffat, A. E. Lutz, G. Dixon-Lewis, M.D. Smooke, J. Warnatz, G.H. Evans, R.S. Larson, R. E. Mitchell, L.R. Petzold, W.C. Reynolds, M. Caracotsios, W.E. Stewart, P. Glarborg, C. Wang, O. Adigun, TRANSPORT-a Software Package For the Evaluation of Gas-Phase, Multicomponent Transport Properties, Reaction Design, Inc., 2000.

[38] J. Sun, Y. Wang, B. Tian, Z. Chen, detonationFoam: an open-source solver for simulation of gaseous detonation based on OpenFOAM, Comput. Phys. Commun. 292 (2023) 108859.

[39] OpenFOAM (2024). https://openfoam.org/.

[40] J. Sun, P. Yang, B. Tian, Z. Chen, Effects of wedge-angle change on the evolution of oblique detonation wave structure, Phys. Fluids 34 (2022) 096112.

[41] J. Sun, P. Yang, B. Tian, Z. Chen, Evolution and control of oblique detonation wave structure in unsteady inflow, AIAA J. 61 (2023) 4808–4820.

[42] B. Van Leer, Towards the ultimate conservative difference scheme. IV. A new approach to numerical convection, J. Comput. Phys. 23 (1977) 276–299.

[43] W. Xie, R. Zhang, J. Lai, H. Li, An accurate and robust HLLC-type Riemann solver for the compressible Euler system at various Mach numbers, Int. J. Numer. Methods Fluids 89 (2018) 430–463.

[44] S.P.N.E. Hairer, G. Wanner, Solving Ordinary Differential Equations II: Stiff and Differential-Algebraic Problems, 2nd ed., Springer-Verlag, Berlin, 1996.

[45] A. Imren, D.C. Haworth, On the merits of extrapolation-based stiff ODE solvers for combustion CFD, Combust. Flame 174 (2016) 1–15.

[46] H. Teng, H.D. Ng, Z. Jiang, Initiation characteristics of wedge-induced oblique detonation waves in a stoichiometric hydrogen-air mixture, Proc. Combust. Inst. 36 (2017) 2735–2742.

[47] L. Srinath, R. Sriram, P. Akhilesh, G. Jagadeesh, Shock-induced leading-edge separation in hypersonic flows, J. Fluid. Mech. 947 (2022) A14.

[48] K. Naidoo, B.W. Skews, Dynamic effects on the transition between two-dimensional regular and Mach reflection of shock waves in an ideal, steady supersonic free stream, J. Fluid. Mech. 676 (2011) 432–460.